

# Constraining Dark Matter distribution in galaxy clusters with MUSE

Baptiste KLEIN \*

*Institut Supérieur de l'aéronautique et de l'Éspace (ISAE), SUPAERO, 31400 Toulouse France*

Jean-Paul KNEIB<sup>†</sup> and Markus REXROTH<sup>‡</sup>

*Laboratoire d'Astrophysique, École Polytechnique Fédérale de Lausanne (EPFL), Observatoire de Sauverny, CH-1290 Versoix, Switzerland*

Clusters of galaxies are the most spectacular gravitational lenses in the universe. They deflect the light rays coming from the galaxies located in their background leading to the creation of numerous multiple images within their cores. These multiple images are used to constrain galaxy cluster dark matter distribution that typically represents  $\sim 80\%$  in such astrophysical objects. High resolution imaging with the Hubble Space Telescope allowed for the identification of a substantial number of strongly lensed objects, leading to precise mass models for a large number of galaxy clusters. Nevertheless, high resolution imaging is not enough and one needs to know the distance of the lensed object, i.e. its redshift, in order to obtain accurate mass models.

The MUSE integral field unit on the VLT is perfectly suited to the observations of galaxy cluster cores where strong lensing is happening. When combined with high resolution images, MUSE observations of a cluster core typically lead to the extraction of more than 150 spectra of sources in the field of view. The analysis of MUSE data cubes allows for the measurement of the spectroscopic redshift of both multiple images and cluster members, thus adding strong constraints to the mass models.

We present the analysis of MUSE observations of MS 0451, MACS J2129 and RX J2129, three galaxy clusters at redshift 0.55, 0.589 and 0.235 respectively. We measured 185, 189 and 158 spectroscopic redshifts among which were 44, 52 and 36 new cluster members and 2, 4 and 3 new systems of multiple images respectively. This resulted in a more accurate mass model for RX J2129 and a deep restructuration - still in progress - of the mass models of the last two clusters. The MUSE and HST data together have been revealed to be one of the most powerful combinations for accurately modeling the dark matter density within galaxy clusters.

## Nomenclature

<i>ACS</i>	=	Advanced Camera for Surveys	<i>WCS</i>	=	World Coordinate System
<i>CLASH</i>	=	Cluster Lensing And Supernova survey with Hubble	<i>WFC3</i>	=	Wide Field Camera 3
<i>dof</i>	=	degree of freedom	<i>c</i>	=	The Speed of light
<i>HFF</i>	=	Hubble Frontier Fields	<i>G</i>	=	Gravitational constant
<i>HST</i>	=	Hubble Space Telescope	<i>pc</i>	=	parsec
$\Lambda$ CDM	=	Lambda Cold Dark Matter model	<i>R</i>	=	Projected radius
<i>MPDAF</i>	=	MUSE Python Data Analysis Framework	<i>z</i>	=	redshift
<i>MUSE</i>	=	Multi-Unit Spectroscopic Explorer	$\sigma$	=	One dimensional velocity dispersion
<i>PIEMD</i>	=	Pseudo Isothermal Elliptical Mass Distribution			
<i>VLT</i>	=	Very Large Telescope			

\*Master's student, baptiste.philippe.klein@gmail.com

<sup>†</sup>Professor at the EPFL, jean-paul.kneib@epfl.ch

<sup>‡</sup>Doctor at the EPFL, markus.rexroth@epfl.ch

## I. Introduction

COSMOLOGY has gone through major evolutions over the last twenty years, mostly due to high precision observations. The surveys of the Cosmic Microwave Background (CMB) spectrum such as the Cosmic Background Explorer (COBE) ([1], [2]) and the Wilkinson Microwave Anisotropy Probe (WMAP) ([3]) were all in agreement with an homogeneous, isotropic and expanding universe without curvature. Measurements of the Hubble diagram of Type Ia supernovas carried out by Perlmutter et al. [4] and Riess et al. [5] were interpreted as an evidence for the acceleration of the expansion of the universe. These major results are consistent with the Lambda Cold Dark Matter model ( $\Lambda$ CDM) which is the current standard model of cosmology. According to the  $\Lambda$ CDM, the matter in the universe is dominated by so-called dark matter which is fundamentally unknown and represents  $\sim 80\%$  of the matter in the universe according to observations by the Planck Satellite ([6]). Dark matter interacts gravitationally with matter and does not emit light, making it difficult to be constrained observationally.

It is however possible to indirectly constrain the dark matter mass distribution in large astrophysical objects using gravitational lensing. As a consequence of General Relativity, the most massive structures in the universe locally deform space-time, thus deflecting the light rays in their vicinity. As the biggest virialized known structures in the universe, clusters of galaxies are the most spectacular gravitational lenses. It is therefore common to observe strongly-lensed images of the galaxies located in the background of galaxy cluster cores, such as giant arcs and multiple images of unique sources. Since gravitational lensing depends only on the total mass of the lens (baryonic and dark), the analysis of the magnified images in a galaxy cluster core is a powerful way to probe its total mass distribution. The fraction of the baryonic mass within a galaxy cluster can be derived from the combination of X-ray observations which probe the cluster gas fraction ([7], [8]) and observations in the visible range which probe the fraction of galaxies, assuming a mass-luminosity relation (e.g. [9], [10]). It is thus possible to subtract the fraction of baryons within the cluster from the total mass distribution to look at dark matter mass distribution only.

The LENSTOOL software uses the observations of multiple images produced by a galaxy cluster to estimate its most likely total mass distribution ([11], [12]). From the location and redshift (i.e. distance) of the multiple images, LENSTOOL uses a Bayesian Markov Chain Monte Carlo (MCMC) to infer the best set of parameters to describe the mass distribution within the cluster (see [12] and the review [13]). Recent surveys with the Hubble Space Telescope (HST) such as the Cluster Lensing And Supernova survey with Hubble (CLASH\*) and the Hubble Frontier Field (HFF<sup>†</sup>) provided deep high-resolution images of galaxy clusters in different filters. This allowed for the identification of a large number of multiple images, substantially increasing the precision of the cluster mass models (e.g. [14], [15], [16], [17]). However, imaging does not allow for a precise measurement of the redshift of the sources which can be derived from their spectrum (see the introduction of [18]). As things stand, the characterization of a consequent number of multiple images could still be completed by adding a spectroscopic redshift. This would decrease the number of free parameters and thus increase the accuracy of the cluster mass models. As precise total mass models are required to constrain the dark matter cross section ([19], [20], [21]), test the cosmological paradigm ([22], [23], [24]) and probe the early universe and reionization (e.g. [25]), it is particularly important to maximize the accuracy and precision of the mass models of a large number of galaxy clusters.

The Multi-Unit Spectroscopic Explorer (MUSE, [26]) is a second generation integral field spectrograph at the Very Large Telescope (VLT). It slices the incoming light into a set of integral field units allowing a spectrum for each pixel of the image to be obtained. MUSE's large field of view of  $1 \text{ arcmin}^2$  is perfectly adapted to the observation of galaxy cluster cores where multiple images are the most likely to form (see the review [27]). Its high sensitivity of between  $4750 \text{ \AA}$  and  $9350 \text{ \AA}$  allows for the detection of sources with redshift up to 6 ([28]). Over the last three years, strong cluster lenses have been observed with MUSE leading to the measurement of spectroscopic redshifts for cluster members and multiple images, improving thus the constraints of the mass models (e.g. [29], [30], [18]).

We present here a MUSE data analysis of three galaxy clusters: MS 0451, MACS J2129 and RX J2129. These three clusters are well-known strong lenses for which a mass model already exists. MS 0451 ( $z = 0.55$ ) is originally known as a strong source of X-rays (see Gioia et al. [31]) but its total mass distribution has been modeled with LENSTOOL by Borys et al. [32] and more recently by MacKenzie et al. [33] thanks to sub-millimeter detections. 9 multiple image systems have already been identified in the south of the cluster, leaving the north poorly constrained. However, a recent work allowed for the identification of 6 new systems of multiple images including a high-redshift quintuple image in the north of the cluster (Kneib et al. in prep.). MACS J2129 ( $z = 0.589$ ) and RX J2129 ( $z = 0.235$ ) are two members of the CLASH survey. The first one was modeled by Monna et al. [34] using CLASH photometry ([35]) and counts 9 multiple images. RX J2129 was modeled with LENSTOOL in Richard et al. [36] using 4 multiple images.

---

\*<https://archive.stsci.edu/prepds/clash/>

†<https://frontierfields.org>

The paper is organized as follows: in Section II, we detail the pipeline that we used to extract as many spectra as possible from MUSE observations. In Section III, we describe the redshift measurement and our results for the three clusters. The strong lensing analysis of the clusters is presented in Section IV and the results are shown in Section V. We conclude in Section VI. Throughout this paper, we assume a standard cosmological model with  $\Omega_M = 0.3$ ,  $\Omega_\Lambda = 0.7$ , and  $H_0 = 70 \text{ km s}^{-1} \text{ Mpc}^{-1}$ . The redshift  $z$  is a consequence of the expansion of the universe and is defined as

$$1 + z = \frac{\lambda_{obs}}{\lambda} \quad (1)$$

where  $\lambda_{obs}$  is the wavelength measured by the observer and  $\lambda$  is the emitted wavelength. At the redshift of MS 0451 ( $z = 0.55$ ), one arcsecond covers a physical distance of 6.412 kpc. For MACS J2129 ( $z = 0.589$ ), one arcsecond corresponds to 6.63 kpc. Finally, at the redshift of RX J2129 ( $z = 0.235$ ), one arcsecond covers a physical distance of 3.3734 kpc. All magnitudes are measured using the AB system.

## II. Data reduction and spectrum extraction

We present here the pipeline that we used in order to maximize the number of extracted spectra from MUSE data cubes. The method is illustrated in Figure 1. Similar methods have been used in Rexroth et al. [37] and in Rexroth et al, 2018 (in prep.).

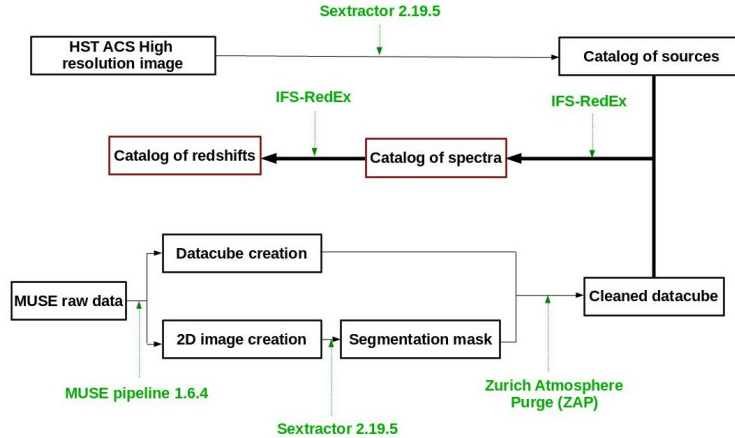


**Fig. 1** Illustration of the pipeline used to extract the spectra from MUSE observations. The manipulated objects are displayed in black boxes and the software packages used are written in green

### A. Data reduction

MS 0451, MACS J2129 and RX J2129 galaxy clusters were observed with MUSE on the VLT. Table 1 shows the observational date, position, ID and time of each exposure. For each of pointing, we took three exposures slightly shifted ( $\sim 0.5$  arcsec) to statistically remove systematics on the detector. The data were taken using MUSE WFM-NOAO-N mode in good seeing conditions with full width at half maximum (FWHM  $\sim 0.6$  arcsec).

The data were reduced using version 1.6.4 of MUSE standard pipeline ([38], [39]). We used a set of standard calibration exposures taken regularly to make bias, arc and flat field master calibration files. Dark current was neglected due to its very low value in the MUSE instrument ( $\approx 1 e^-/h$ ; [28]). We first subtracted bias images from each dataset and performed an illumination correction using both the flat field master file and the twilight sky exposure which were taken soon before/after the science observations. We carried out geometrical and astrometric calibrations in order to assign the *World Coordinate System* (WCS) right ascension and declination and the wavelength to each spaxel of the data cube. The flux calibration was carried out using standard candles in the field of view. For each pointing of each cluster, the three individual exposures were finally combined into a single data cube.

We applied the Zürich Atmosphere Purge (ZAP; [40]) to subtract the sky residuals within each data cube. This method requires a segmentation mask created by the SExtractor software ([41]) when running on the collapsed data cube along its wavelength axis. ZAP uses the mask to remove the principal visible sources from the data cube, leading to a data cube dominated by the sky signal. For each spectral plane, the median is calculated and subtracted, providing thus a data cube with sky and astronomic residuals only. ZAP then applies a principal component analysis to this data

**Table 1** Summary of the main information about MUSE observations of the clusters. The Right Ascension (RA) and DEClination (DEC) are displayed in column (7) and (8).

Name	$z$	ESO program	PI	Exposure time [s]	Observation dates	RA [deg J2000]	DEC [deg J2000]
MS0451	0.55	096.A-0105(A)	JP Kneib	1447	2016-01-10	73.551654	-3.01837
					2016-01-11	73.541064	-3.00965
MACS2129	0.59	095.A-0525(A)	JP Kneib	1462	2015-06-17	322.366021	-7.6904
					2015-06-17	322.351921	-7.6904
RXJ2129	0.23	097.A-0909(A)	JP Kneib	1490	2016-08-05	322.421488	0.09307
					2016-09-04	322.411888	0.08682

cube and creates a new data cube using the minimum of eigenspectra in order to keep all the astronomical signals while removing most of the sky signal. The final data cube corresponds to the combination of this reconstruction and of the signal removed with the segmentation mask.

The wavelength range of the final data cube stretches from 4750 Å to 9350 Å in steps of 1.25 Å and the pixel size is 0.2 arcsec.

## B. Spectrum extraction

We combined MUSE observations with HST high resolution images leading us to detect small and faint sources invisible in the image obtained when the data cube is collapsed along the wavelength axis. This combination was notably used by Bacon et al. [28] for the analysis of MUSE observations of the Hubble Deep Field South.

For the MACS J2129 and RX J2129 galaxy clusters, we used HST data obtained with the Advanced Camera for Surveys (ACS<sup>‡</sup>; [42]) in the frame of the CLASH survey in the bands F475W, F625W and F814W. We also used the Wide Field Camera 3 (WFC3<sup>§</sup>) in the bands F110W and F160W in order to maximize the number of detected sources. For MS 0451, we used the HST data available in MAST website<sup>¶</sup> ([43]).

We used IFS-REDEX software to align the data cubes with the corresponding high resolution images ([37]). The source extraction was carried out with the application of SEXTRACTOR to the high resolution image in the F814W band. IFS-REDEX uses the catalog of detected sources to extract the signal in the data cube within a circle with a radius of 3 to 5 pixels according to the FWHM measurement. The sources with FWHM < 2 are regarded as spurious detections and are not extracted.

In order to maximize the number of extracted spectra, we carried out a blind search in the data cube using MUSELET<sup>||</sup>. This software is part of the MUSE Python Data Analysis Framework (MPDAF; [44]). It builds a new data cube, the narrow-band data cube, within which each wavelength plane is the mean of the 5 closest wavelength planes in the science data cube. MUSELET then uses SEXTRACTOR to extract a catalog of sources at each wavelength of the narrow-band data cube. The latter are finally merged and sorted, leading to the creation of continuum and single-line emission catalogs.

Finally, all the catalogs are merged into a master catalog and displayed in the high-resolution image so that the user can determine whether MUSELET and SEXTRACTOR detections are part of the same source. This results in a set of spectra that will be analyzed in order to measure the redshift of the associated sources.

## III. Redshift measurement

### A. Method

IFS-REDEX comes up with an interactive interface which displays each extracted spectrum and the corresponding source in SAODS9 ([45]). It allows the user to modify the source redshift to fit an emission/absorption line template to its most likely position in the spectrum. To simplify the redshift identification, it is possible to smooth the signal with a Gaussian filter and to perform a wavelet-based spectrum cleaning [37]. The systematic error is calculated by adding the

<sup>‡</sup>List of ACS filters : [http://www.stsci.edu/hst/acs/documents/handbooks/current/c05\\$\\_imaging2.html](http://www.stsci.edu/hst/acs/documents/handbooks/current/c05$_imaging2.html)

<sup>§</sup><https://wfc3.gsfc.nasa.gov>

<sup>¶</sup><http://archive.stsci.edu/>

<sup>||</sup><http://mpdaf.readthedocs.io/en/latest/muselet.html>

wavelength calibration error provided by the MUSE data reduction pipeline to the error given by fitting a Gaussian to the most prominent line in the spectrum. To each redshift, we assigned a quality flag which was set to 3 if the redshift was secure, 2 if likely (e.g. one line only), 1 if insecure and 0 otherwise.

We sequentially analyzed all the extracted spectra in the three galaxy clusters. Most of the extracted spectra present characteristic ultraviolet lines shifted into the visible range. We noticed a small number of stars ( $z = 0$ ) and  $H\alpha$  emitters in the foreground of the clusters ( $z \leq 0.3$ ) and a large amount of absorption galaxies that belong to the clusters. Most of the galaxies detected behind the clusters presented strong emission lines such as OII duplets ( $0.5 \leq z \leq 1.5$ ) and  $Ly\alpha$  lines ( $3.0 \leq z \leq 6.0$ ). The measured redshifts were sorted depending on whether they belong to a source located in the foreground of the cluster, in the cluster itself or in the background of the cluster.

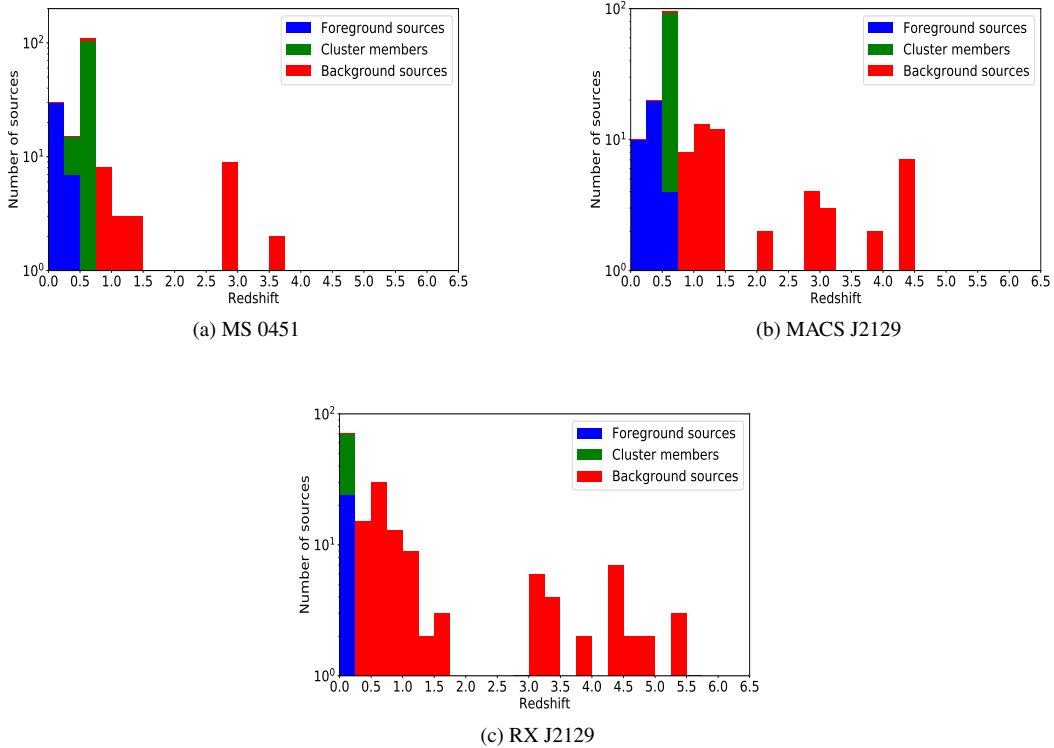


**Fig. 2** Source distributions from MUSE extraction in redshift space for MS0451 (a), MACS2129 (b) and RXJ2129 (c).

## B. Results of the redshift extraction

Figure 2 shows the histograms of the redshifts extracted from MUSE data cubes for the three galaxy clusters.

- *MS 0451*: We extracted 185 sources with redshifts ranging from 0.0 to 4.85. Among them, 112 are cluster members with  $0.52 < z < 0.58$ , 38 sources are located in the foreground of the cluster and 35 in the background of the cluster.
- *MACS J2129*: We extracted 189 sources with redshifts ranging from 0.0 to 4.92. Among them, 89 are cluster members with  $0.56 < z < 0.62$ , 39 sources are located in the foreground of the cluster and 61 in the background of the cluster.
- *RX J2129*: We extracted 158 sources with redshifts ranging from 0.0 to 5.53. Among them, 43 are cluster members with  $0.21 < z < 0.25$ , 24 are located in the foreground of the cluster and 91 in the background of the cluster.

## IV. Strong lensing analysis

We used LENSTOOL software ([11], [12]) to perform a strong lensing analysis of MS 0451, MACS J2129 and RX J2129. We started from previous strong lensing models and used the newly measured redshifts to carry out the identification of new cluster members and multiple image systems and to add spectroscopic redshifts when missing.

### A. Model of mass distribution

Similarly to Jullo et al. [12], we decompose the gravitational potential of the galaxy cluster into large scale halo and sub-halo potentials,  $\Phi_{c_i}$  and  $\Phi_{p_j}$  such that

$$\Phi_{tot} = \sum_i \Phi_{c_i} + \sum_j \Phi_{p_j} \quad (2)$$

Assuming that the clusters can be described as two dimensional structures according to the thin lens approximation (see the review [27]), we model the mass distribution of each halo through a Pseudo Isothermal Elliptical Mass Distribution (PIEMD; [46], [47], [48]):

$$\Sigma(R) = \frac{\sigma^2}{2G} \frac{r_t}{r_t - r_c} \left( \frac{1}{\sqrt{R^2 + r_c^2}} - \frac{1}{\sqrt{R^2 + r_t^2}} \right) \quad (3)$$

where a core radius  $r_c$  and a truncation radius  $r_t$  are used. The projected radius  $R^2 = x^2/(1+e)^2 + y^2/(1-e)^2$  is defined using the relation  $e = (a-b)/(a+b)$ , the module of the complex ellipticity defined in Natarajan and Kneib [49].  $x$  and  $y$  are defined with respect to the position of the center of the mass distribution. In practice  $e = e \times e^{2i\theta}$  where  $\theta$  is the orientation angle of the ellipse seen from the observer point of view with respect to the north.  $a$  and  $b$  are respectively the semi-major and semi-minor axes of the mass distribution.  $\sigma$  stands for the one dimensional velocity dispersion. The position of the center, the ellipticity, the truncation and core radii and the velocity dispersion are the height parameters needed to describe a mass distribution with the PIEMD model. The surface mass density of each halo  $\Sigma_i(R)$  is linked to its gravitational potential  $\Phi_i(R)$  thanks to the Poisson equation:

$$4\pi G \Sigma_i(R) = \nabla^2 \Phi_i(R) \quad (4)$$

As pointed out in Jullo et al. [12], the optimization of height parameters per sub-halo would lead to an under-constrained problem. We thus assume that we can trace mass with luminosity in each cluster galaxy (see the discussion in [50]). Therefore we assimilate the sub-halo position and ellipticity to their luminous counterpart and scale  $\sigma$ ,  $r_c$  and  $r_t$  thanks to a reference galaxy in the cluster.

### B. Strong lensing modeling with LENSTOOL

LENSTOOL uses the position and redshift of the multiple images to constrain the parameters of the mass distribution with respect to the so-called lens equation ([51]):

$$\boldsymbol{\beta} = \boldsymbol{\theta} - \frac{D_{ds}}{D_s} \boldsymbol{\alpha}(\boldsymbol{\theta}) \quad (5)$$

where  $\boldsymbol{\beta}$  is the angular position (right ascension and declination) of the source,  $\boldsymbol{\theta}$  is the angular position of the image of the source in the cluster plane and  $D_{ds}$  and  $D_s$  are respectively the distances between the lens and the source and between the observer and the source.  $\boldsymbol{\alpha}$  is the deflection angle such that

$$\boldsymbol{\alpha}(\mathbf{b}) = \frac{4G}{c^2} \int_{\mathbb{R}^2} \Sigma(\mathbf{b}') \frac{\mathbf{b} - \mathbf{b}'}{|\mathbf{b} - \mathbf{b}'|^2} d^2 \mathbf{b}' \quad (6)$$

where  $\mathbf{b}$  is the impact parameter defined from the barycenter of the mass distribution of the cluster.

In practice, we access only the position of the multiple images within the cluster and the position of the source is unknown. For each multiple image, LENSTOOL computes the position of the associated source given the mass distribution. For each system of multiple images, it takes the barycenter of the predicted sources in the source plane and uses lens equation 5 to predict the theoretical position of the multiple images given the mass distribution. The accuracy of a given mass distribution is computed thanks to a  $\chi^2$ :

$$\chi^2 = \sum_i \chi_i^2 \quad (7)$$

where the  $i$  index refers to the system of multiple images and  $\chi_i^2$  is such that:

$$\chi_i^2 = \sum_{j=1}^{n_i} \frac{(\theta_{obs}^j - \theta^j(\mathbf{p}))^2}{\sigma_{ij}^2} \quad (8)$$

where  $\theta_{obs}^j$  is the observed position of the multiple image  $j$ ,  $\theta^j$  is the predicted position of the multiple image  $j$  given the model,  $n_i$  is the number of multiple images in system  $i$  and  $\sigma_{ij}$  is the error in the position of image  $j$ . `LENSTOOL` carries out a Bayesian  $\chi^2$  minimization with a MCMC sampling of the parameter space. The quality of the best model is assessed thanks to its  $\chi^2$  value and the root mean square (rms) error between the observed multiple images and their predicted position given the model.

### C. Cluster member and multiple image selection

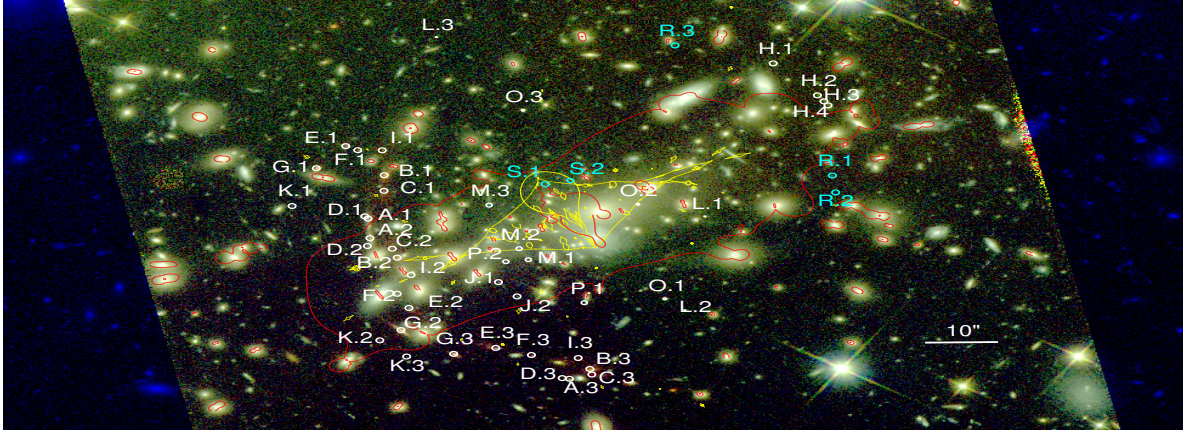
We compared our catalogs of sources located in the clusters and in their background to the list of sub-halos and multiple images used in the reference mass models of the three galaxy clusters. We added the new cluster members as sub-halo potentials to the previous models and added a spectroscopic redshift to the multiple images when possible. We also carried out a search for new multiple images with our catalogs of background sources. We used the reference model of each cluster to predict the multiplicity of the sources located in the background of the cluster. In parallel, we searched for multiple images in HST high resolution images in a wide range of filters and analyzed the narrow-band data cubes in the wavelengths corresponding to the maximum emission of each background source. When confirmed, the new multiple image system was added to the model which was computed in a computer cluster (1node, 16 cores) and compared to the previous one.

- *MS 0451*: We started from the model of MacKenzie et al. [33] recently revised thanks to, inter alia, a  $z = 6.7$  quintuple image located in the poorly-constrained north region of the cluster (Kneib et al. in prep.). We report the identification of two systems of multiple images at high redshift. System R ( $z = 3.7645$ ) is a triple image in the north of the cluster and system S ( $z = 4.4514$ ) is also triply-imaged but with only two identified images. We also report the measurement of a spectroscopic redshift of  $z = 2.92$  for system G and the detection of 44 new cluster members.
- *MACS J2129*: We adapted the model of Monna et al. [34] based on Zitrin et al. [52] strong lensing method into a `LENSTOOL` model. We report the identification of four multiple image systems. Systems 10, 11 and 12, with redshifts of  $z = 4.41$ ,  $z = 3.1081$  and  $z = 3.897$  respectively, are triply-imaged systems for which only two multiple images could be detected. System 13,  $z = 1.3585$  is a totally identified triple image. We also found a redshift of  $z = 1.357$  for System 7 and report the identification of 52 new cluster members.
- *RX J2129*: We started from the `LENSTOOL` parametric model from Richard et al. [36]. We report the identification of three new multiple image systems. Systems 6 ( $z = 0.6786$ ) and 8 ( $z = 1.52$ ) which are confirmed triply-imaged systems and System 7 ( $z = 3.08$ ) for which we could only identify two multiple images among the three predicted by the model. We also determined a spectroscopic redshift for Systems 5 ( $z = 0.916$ ) and 3 ( $z = 1.52$ ), and confirmed the redshifts of systems 1 and 2.

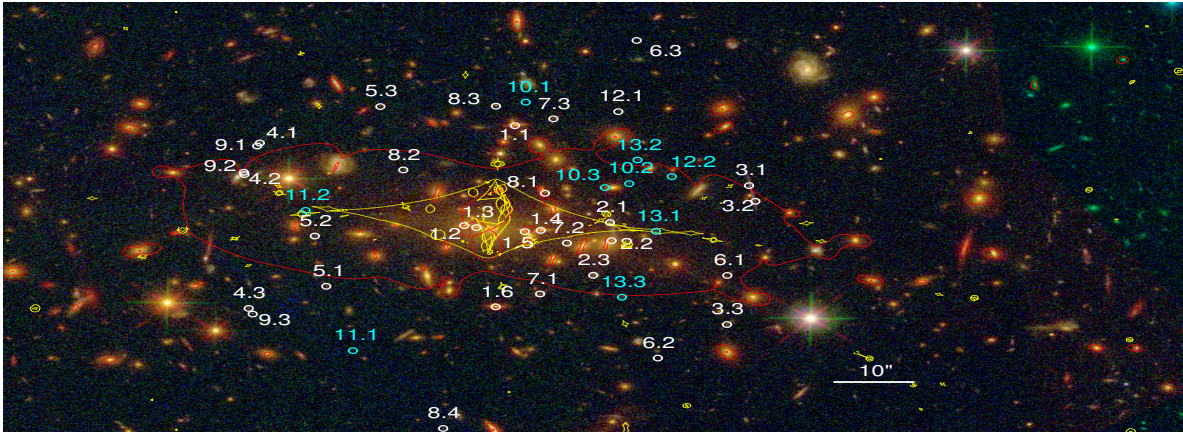
## V. Results and discussion

We used `LENSTOOL` to carry out the  $\chi^2$  minimization for MS 0451, MACS J2129 and RX J2129 mass models. The multiple images used in the models are displayed in Figure 3.

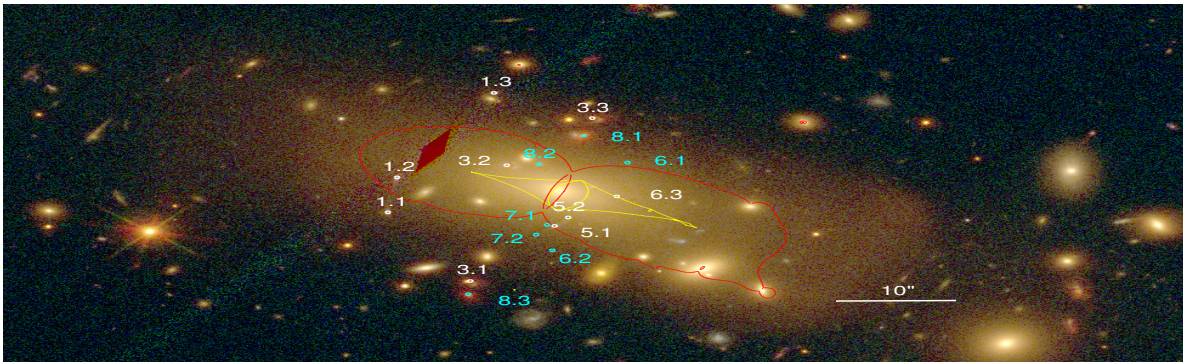
- *RX J2129*: We obtained a mass model with a  $\chi^2$  of 4.7 for 17 degrees of freedom (dof) and a median rms error of 0.24 arcsec which has to be compared to a  $\chi^2$  of 3 with 5 degrees of freedom and a rms of 0.05 arcsec. The rise in the median rms is explained by the very low number of multiple images and cluster members used in the reference model. The increase in the number of constraints due to the doubling of the number of multiple images and cluster members improved the accuracy of the model symbolized by the decrease of  $\chi^2/dof$ . The contours of the mass distribution and the integrated mass profile are shown in Figure 4. We notice deep changes in the contours of the mass distribution. The addition of new cluster members modifies locally the mass distribution, as can be seen in the south-east part of the cluster core. Moreover, the bias between the contours of the reference and MUSE-based models can be explained by the addition of new multiple images to the model. Last but not least, there is a net difference between the slopes of the integrated mass profiles not least in the vicinity of the center of the cluster.
- *MACS J2129*: We obtained a  $\chi^2/dof$  of 165/40 with a median rms error of 1.01 arcsec which has to be compared to a  $\chi^2/dof$  of 29/21 with a median rms of 0.4 arcsec. The analysis of this strong difference reveals that three images from Monna et al. [34] are poorly reproduced by the model with an error greater than 2 arcsec. A deeper



(a) The core of MS 0451 on a RGB infrared image with HST ACS F814W (blue), F110W (green), F160W (red) filters. Critical lines and caustics are displayed at  $z = 2.9$ .

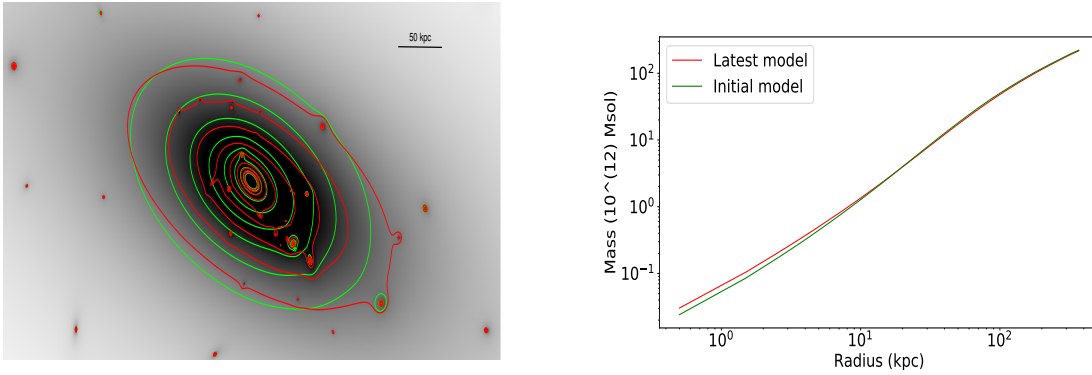


(b) The core of MACS J2129 on a RGB image with HST ACS F475W (blue), F625W (green), F814W (red) filters. Critical lines and caustics at  $z = 2.0$ .



(c) The core of RX J2129 on a RGB image with HST ACS F475W (blue), F625W (green), F814W (red) filters. Critical lines and caustics at  $z = 1.4$ .

**Fig. 3** Display of the upgraded list of multiple images in MS 0451 (a), MACS J2129 (b) and RX J2129 (c) models on a HST image. The critical and caustic lines, i.e. the lines of infinite magnification at a given redshift, are drawn in red and yellow respectively at a characteristic  $z$ . The multiple images are flagged by a circle which is cyan if the system was added thanks to MUSE data and white otherwise. For RX J2129, multiple system 2 is located at  $\sim 300$  kpc, i.e. 80 arcsec from the center of the cluster and is not displayed here.



(a) RX J2129: Contours are shown in steps of  $1 \times 10^{10} M_{\odot}/kpc$  starting from  $3.7 \times 10^{10} M_{\odot}/kpc$ . Contours are displayed in green when from the initial model from Richard et al. [36] and in red when from the last improved model

(b) Comparison between RX J2129 integrated mass profiles defined from the center of the cluster. The mass profile is displayed in green when from the reference model and in red when from the model updated with MUSE data

**Fig. 4 Integrated mass distribution (a) and integrated mass profile (b) of RX J2129 and comparison to the reference model**

investigation of this difference is currently being carried out in the Geneva Observatory. Since all the poorly reproduced multiple images are located in the same region of the cluster and have been individually confirmed, we suggest that this difference is due to a second large scale dark matter halo in this region. Therefore we have started to compute another model (ongoing) which includes the optimization a second large scale halo.

- *MS 0451*: We obtained a  $\chi^2$  of 122/39 with a total rms of 0.79 arcsec. As mentioned above the south of the cluster is well constrained whereas the north is almost empty. Therefore, the addition from Kneib et al. (in prep.) of a quintuple image at  $z = 6.7$  (system H) makes it difficult to obtain a low  $\chi^2$  value. Moreover, multiple images H.2, H.3 and H.4 are very close (within a few arcsec) and the current version of LENSTOOL is not precise enough to correctly compute the magnification map in the source plane at the redshift of H. The addition of Systems R and S and the cluster members from MUSE data analysis does not improve the quality of the model. However, the presence of two groups in the vicinity of System H could be symptomatic of isolated dark matter halos that could locally increase the magnification of the galaxies located in the background. Moreover, a closer look to the MUSE data revealed an unidentified cluster member invisible in the HST images and located in the vicinity of Image R.1. We have thus computed two models (ongoing) including the optimization of the parameters of respectively one and two dark matter halos and the invisible cluster member. Preliminary results seem to be in agreement with these models with a substantial decrease in the median rms ( $\sim 0.55$  arcsec).

## VI. Conclusions

In this paper, we have presented a new mass model for three galaxy clusters: two CLASH clusters, MACS J2129 and RX J2129, and MS 0451. We combined MUSE integral field units with high resolution images from the HST in order to maximize the number of extracted sources. We measured the redshift of each source with dedicated software, IFS-REDEX, allowing for a wavelet-based filtration of the spectra. Our main conclusions for this study are as follows:

- We measured 185, 189 and 158 secure or likely redshifts for MS 0451, MACS J2129 and RX J2129 respectively. For MS 0451, we identified two new systems of multiple images, confirmed the redshift of the giant arc from [32] and measured the redshift of the three multiple images of System G. For MACS J2129, we identified four new systems of multiple images, confirmed the redshift of Systems 1, 2, 3 and 8 and measured a spectroscopic redshift of System 7. For RX J2129, we almost doubled the number of constraints by adding three new systems of multiple images and measuring the redshift of all the systems of [36] model. We finally added 44, 52 and 36 cluster members for MS451-03, MACS J2129 and RX J2129 respectively.
- The combination of high resolution imaging and integral field spectroscopy turned out to be an efficient method for detecting new multiple image systems and cluster members. In the frame of this work, this led to sharply different mass models for RXJ2129 and revealed possible dark matter sub-halos in the two other clusters which opens the door to interesting further work.

Similarly to Richard et al. [29] and Lagattuta et al. [18], these results corroborate the strong value of MUSE integral field units for cluster lensing. Beyond the creation of expanded redshift catalogs, MUSE allows for the identification of new multiple images and cluster members which are mandatory to increase the accuracy of the cluster mass models.

## Acknowledgments

I would like to thank my advisors, Prof. Jean-Paul KNEIB and Dr. Markus REXROTH for their precious help, availability and advice throughout this Master's internship. My sincere gratitude goes also to Dr. Mathilde JAUZAC (Durham University), Dr. Johan RICHARD (CRAL, Lyon) and Christophe SCHAFFER for their interest and implication in this project. I would like to address special thanks to Aurélien VERDIER, whom I supervised during his summer internship and who helped me to go faster in the redshift extraction. Finally, I am grateful to all the personal of the Geneva Observatory for their warm welcome.

## References

- [1] Mather, J. C., et al., "A preliminary measurement of the cosmic microwave background spectrum by the Cosmic Background Explorer (COBE) satellite," *ApJ*, Vol. 354, 1990, pp. L37–L40. doi:10.1086/185717.
- [2] Smoot, G. F., Bennett, C. L., Kogut, A., et al., "Structure in the COBE differential microwave radiometer first-year maps," *ApJ*, Vol. 396, 1992, pp. L1–L5. doi:10.1086/186504.
- [3] Bennett, C. L., et al., "First-Year Wilkinson Microwave Anisotropy Probe (WMAP) Observations: Preliminary Maps and Basic Results," *ApJS*, Vol. 148, 2003, pp. 1–27. doi:10.1086/377253.
- [4] Perlmutter, S., Gali, S., et al., "Measurements of the Cosmological Parameters  $\Omega$  and  $\Lambda$  from the First Seven Supernovae at  $z \geq 0.35$ ," *ApJ*, Vol. 483, 1997, pp. 565–581. doi:10.1086/304265.
- [5] Riess, A. G., et al., "Observational Evidence from Supernovae for an Accelerating Universe and a Cosmological Constant," *AJ*, Vol. 116, 1998, pp. 1009–1038. doi:10.1086/300499.
- [6] Planck Collaboration, et al., "Planck 2015 results. XIII. Cosmological parameters," *A&A*, Vol. 594, 2016, A13. doi:10.1051/0004-6361/201525830.
- [7] Lea, S. M., Silk, J., Kellogg, E., and Murray, S., "Thermal-Bremsstrahlung Interpretation of Cluster X-Ray Sources," *ApJ*, Vol. 184, 1973, p. L105. doi:10.1086/181300.
- [8] Eckert, D., et al., "The XXL Survey. XIII. Baryon content of the bright cluster sample," *A&A*, Vol. 592, 2016, A12. doi:10.1051/0004-6361/201527293.
- [9] Faber, S. M., and Jackson, R. E., "Velocity dispersions and mass-to-light ratios for elliptical galaxies," *ApJ*, Vol. 204, 1976, pp. 668–683. doi:10.1086/154215.
- [10] Tully, R. B., and Fisher, J. R., "A new method of determining distances to galaxies," *A&A*, Vol. 54, 1977, pp. 661–673.
- [11] Kneib, J.-P., Ellis, R. S., et al., "Hubble Space Telescope Observations of the Lensing Cluster Abell 2218," *ApJ*, Vol. 471, 1996, p. 643. doi:10.1086/177995.
- [12] Jullo, E., Kneib, J.-P., et al., "A Bayesian approach to strong lensing modelling of galaxy clusters," *New Journal of Physics*, Vol. 9, 2007, p. 447. doi:10.1088/1367-2630/9/12/447.
- [13] Sharma, S., "Markov Chain Monte Carlo Methods for Bayesian Data Analysis in Astronomy," *ArXiv e-prints*, 2017.
- [14] Richard, J., Jauzac, M., Limousin, M., et al., "Mass and magnification maps for the Hubble Space Telescope Frontier Fields clusters: implications for high-redshift studies," *MNRAS*, Vol. 444, 2014, pp. 268–289. doi:10.1093/mnras/stu1395.
- [15] Jauzac, M., Richard, J., et al., "Hubble Frontier Fields: a high-precision strong-lensing analysis of the massive galaxy cluster Abell 2744 using 180 multiple images," *MNRAS*, Vol. 452, 2015, pp. 1437–1446. doi:10.1093/mnras/stv1402.
- [16] Zitrin, A., and others., "Hubble Space Telescope Combined Strong and Weak Lensing Analysis of the CLASH Sample: Mass and Magnification Models and Systematic Uncertainties," *ApJ*, Vol. 801, 2015, 44. doi:10.1088/0004-637X/801/1/44.
- [17] Molino, A., et al., "CLASH: accurate photometric redshifts with 14 HST bands in massive galaxy cluster cores," *MNRAS*, Vol. 470, 2017, pp. 95–113. doi:10.1093/mnras/stx1243.
- [18] Lagattuta, D. J., Richard, J., et al., "Lens modelling Abell 370: crowning the final frontier field with MUSE," *MNRAS*, Vol. 469, 2017, pp. 3946–3964. doi:10.1093/mnras/stx1079.
- [19] Harvey, D., et al., "On the cross-section of dark matter using substructure infall into galaxy clusters," *MNRAS*, Vol. 441, 2014, pp. 404–416. doi:10.1093/mnras/stu337.
- [20] Harvey, D., et al., "The nongravitational interactions of dark matter in colliding galaxy clusters," *Science*, Vol. 347, 2015, pp. 1462–1465. doi:10.1126/science.1261381.
- [21] Wittman, D., Golovich, N., and Dawson, W. A., "The Mismeasure of Mergers: Revised Limits on Self-interacting Dark Matter in Merging Galaxy Clusters," *ArXiv e-prints*, 2017.
- [22] Jullo, E., Natarajan, P., et al., "Cosmological Constraints from Strong Gravitational Lensing in Clusters of Galaxies," *Science*, Vol. 329, 2010, pp. 924–927. doi:10.1126/science.1185759.
- [23] Acebron, A., Jullo, E., et al., "Hubble Frontier Fields: systematic errors in strong lensing models of galaxy clusters - implications for cosmography," *MNRAS*, Vol. 470, 2017, pp. 1809–1825. doi:10.1093/mnras/stx1330.

- [24] Natarajan, P., et al., “Mapping substructure in the HST Frontier Fields cluster lenses and in cosmological simulations,” *MNRAS*, Vol. 468, 2017, pp. 1962–1980. doi:10.1093/mnras/stw3385.
- [25] Atek, H., et al., “Are Ultra-faint Galaxies at  $z = 6-8$  Responsible for Cosmic Reionization? Combined Constraints from the Hubble Frontier Fields Clusters and Parallels,” *ApJ*, Vol. 814, 2015, 69. doi:10.1088/0004-637X/814/1/69.
- [26] Bacon, R., et al., “The MUSE second-generation VLT instrument,” *Ground-based and Airborne Instrumentation for Astronomy III*, Proc. SPIE, Vol. 7735, 2010, p. 773508. doi:10.1117/12.856027.
- [27] Kneib, J.-P., and Natarajan, P., “Cluster lenses,” *A&ARv*, Vol. 19, 2011, 47. doi:10.1007/s00159-011-0047-3.
- [28] Bacon, R., et al., “The MUSE 3D view of the Hubble Deep Field South,” *A&A*, Vol. 575, 2015, A75. doi:10.1051/0004-6361/201425419.
- [29] Richard, J., et al., “MUSE observations of the lensing cluster SMACSJ2031.8-4036: new constraints on the mass distribution in the cluster core,” *MNRAS*, Vol. 446, 2015, pp. L16–L20. doi:10.1093/mnras/lu150.
- [30] Jauzac, M., Richard, J., et al., “Hubble Frontier Fields: predictions for the return of SN Refsdal with the MUSE and GMOS spectrographs,” *MNRAS*, Vol. 457, 2016, pp. 2029–2042. doi:10.1093/mnras/stw069.
- [31] Gioia, I. M., et al., “The Einstein Observatory Extended Medium-Sensitivity Survey. I - X-ray data and analysis,” *ApJS*, Vol. 72, 1990, pp. 567–619. doi:10.1086/191426.
- [32] Borys, C., Chapman, S., et al., “The nature of a gravitationally lensed submillimetre arc in MS0451.6-0305: two interacting galaxies at  $z \sim 2.9$ ?” *MNRAS*, Vol. 352, 2004, pp. 759–767. doi:10.1111/j.1365-2966.2004.07982.x.
- [33] MacKenzie, T. P., Scott, D., et al., “Disentangling a group of lensed submm galaxies at  $z \sim 2.9$ ,” *MNRAS*, Vol. 445, 2014, pp. 201–212. doi:10.1093/mnras/stu1623.
- [34] Monna, A., et al., “Precise strong lensing mass profile of the CLASH galaxy cluster MACS 2129,” *MNRAS*, Vol. 466, 2017, pp. 4094–4106. doi:10.1093/mnras/stx015.
- [35] Zitrin, A., et al., “Hubble Space Telescope Combined Strong and Weak Lensing Analysis of the CLASH Sample: Mass and Magnification Models and Systematic Uncertainties,” *ApJ*, Vol. 801, 2015, 44. doi:10.1088/0004-637X/801/1/44.
- [36] Richard, J., Smith, G. P., et al., “LoCuSS: first results from strong-lensing analysis of 20 massive galaxy clusters at  $z = 0.2$ ,” *MNRAS*, Vol. 404, 2010, pp. 325–349. doi:10.1111/j.1365-2966.2009.16274.x.
- [37] Rexroth, M., Kneib, J.-P., et al., “IFS-RedEx, a redshift extraction software for integral-field spectrographs: Application to MUSE data,” *ArXiv e-prints*, 2017.
- [38] Weilbacher, P. M., et al., “The MUSE Data Reduction Pipeline: Status after Preliminary Acceptance Europe,” *Astronomical Data Analysis Software and Systems XXIII*, Astronomical Society of the Pacific Conference Series, Vol. 485, edited by N. Manset and P. Forshay, 2014, p. 451.
- [39] Weilbacher, P. M., et al., “Design and capabilities of the MUSE data reduction software and pipeline,” *Software and Cyberinfrastructure for Astronomy II*, Proc. SPIE, Vol. 8451, 2012, p. 84510B. doi:10.1117/12.925114.
- [40] Soto, K. T., et al., “ZAP - enhanced PCA sky subtraction for integral field spectroscopy,” *MNRAS*, Vol. 458, 2016, pp. 3210–3220. doi:10.1093/mnras/stw474.
- [41] Bertin, E., and Arnouts, S., “SExtractor: Software for source extraction.” *A&AS*, Vol. 117, 1996, pp. 393–404. doi:10.1051/aas:1996164.
- [42] Ford, H. C., et al., “Overview of the Advanced Camera for Surveys on-orbit performance,” *Future EUV/UV and Visible Space Astrophysics Missions and Instrumentation.*, Proc. SPIE, Vol. 4854, edited by J. C. Blades and O. H. W. Siegmund, 2003, pp. 81–94. doi:10.1117/12.460040.
- [43] Ebeling, H., Edge, A. C., and Henry, J. P., “MACS: A Quest for the Most Massive Galaxy Clusters in the Universe,” *ApJ*, Vol. 553, 2001, pp. 668–676. doi:10.1086/320958.
- [44] Bacon, R., et al., “MPDAF: MUSE Python Data Analysis Framework,” *Astrophysics Source Code Library*, Nov. 2016.
- [45] Joye, W. A., and Mandel, E., “New Features of SAOImage DS9,” *Astronomical Data Analysis Software and Systems XII*, Astronomical Society of the Pacific Conference Series, Vol. 295, edited by H. E. Payne, R. I. Jedrzejewski, and R. N. Hook, 2003, p. 489.
- [46] Elíasdóttir, Á., Limousin, M., et al., “Where is the matter in the Merging Cluster Abell 2218?” *ArXiv e-prints*, 2007.
- [47] Limousin, M., Kneib, J.-P., and Natarajan, P., “Constraining the mass distribution of galaxies using galaxy-galaxy lensing in clusters and in the field,” *MNRAS*, Vol. 356, 2005, pp. 309–322. doi:10.1111/j.1365-2966.2004.08449.x.
- [48] Kassiola, A., and Kovner, I., “Elliptic Mass Distributions versus Elliptic Potentials in Gravitational Lenses,” *ApJ*, Vol. 417, 1993, p. 450. doi:10.1086/173325.
- [49] Natarajan, P., and Kneib, J.-P., “Lensing by galaxy haloes in clusters of galaxies,” *MNRAS*, Vol. 287, 1997, pp. 833–847. doi:10.1093/mnras/287.4.833.
- [50] Harvey, D., Kneib, J. P., and Jauzac, M., “Systematic or signal? How dark matter misalignments can bias strong lensing models of galaxy clusters,” *MNRAS*, Vol. 458, 2016, pp. 660–665. doi:10.1093/mnras/stw295.
- [51] Schneider, P., Ehlers, J., Falco, E. E., and Bleyer, U., “Book-Review - Gravitational Lenses,” *Astronomische Nachrichten*, Vol. 314, 1993, p. 314. doi:10.1002/asna.2113140414.
- [52] Zitrin, A., et al., “The Cluster Lensing and Supernova Survey with Hubble (CLASH): Strong-lensing Analysis of A383 from 16-band HST/WFC3/ACS Imaging,” *ApJ*, Vol. 742, 2011, 117. doi:10.1088/0004-637X/742/2/117.